



## Research Paper

# Maximising the potential of deep geothermal energy: Thermal output increase by large-scale heat pumps

Jaromir Jeßberger<sup>\*</sup>, Florian Heberle, Dieter Brüggemann

Chair of Engineering Thermodynamics and Transport Processes (LTTT), Center of Energy Technology (ZET), University of Bayreuth, Prof.-Rüdiger-Bormann-Strasse 1, DE-95447 Bayreuth, Germany



## ARTICLE INFO

## Keywords:

Large-scale Heat Pump  
Geothermal  
District Heating  
Techno-economic Analysis  
Experimental investigation  
Part load operation

## ABSTRACT

Due to the high share of the heating market in Europe's final energy consumption, it is mandatory to intensify the decarbonisation in this sector. Large-scale heat pumps could significantly contribute to different areas of application, like the supply of existing heating networks or the utilisation of industrial waste heat, by using various energy sources like geothermal, air or running water. However, there are still open research questions regarding the technical aspects like fluid selection or part load behaviour as well as economic aspects.

This study investigates the potential of maximising the thermal capacity of existing geothermal heating plants by integrating large-scale heat pumps. To consider a realistic performance of the heat pump, experimental results are implemented into a techno-economic model. Annual simulations are carried out based on real data for a district heating network and the geothermal source. The experimental investigations of a high-temperature heat pump show the high impact of temperature lift, temperature glides and part load operation on the *COP*. Additionally, this investigated part load behaviour is implemented in the techno-economic model.

For the techno-economic analyses, the levelized costs of heat (*LCOH*) are calculated. For a base scenario, 68 €/MWh are estimated. Additionally, sensitivity analyses were conducted to quantify the influence of selected geological, design and economic parameters on the *LCOH*. The electricity price shows the most significant impact, with a potential reduction of the *LCOH* of 39%. In general, the study points out the great potential of integrating large-scale heat pumps into geothermal energy systems and district heating networks to extend the renewable system's thermal capacity efficiently and cost-effectively.

## 1. Introduction

Reducing global warming through the decarbonisation of the energy sector is one of the biggest challenges of our time. However, renewable energy sources still play a minor role in the heating sector, with about 23% in 2021, although this sector accounts for over 50% of European final energy consumption [1]. Integrating large-scale and high-temperature heat pumps (HTHPs) into renewable energy systems is a promising approach to provide thermal energy in a sustainable and resource-efficient way. Potential applications are geothermal systems or upgrading waste heat from industrial processes. Using HTHPs offers the possibility to ensure sustainable peak load coverage, increase the thermal output of different systems, or raise supply temperatures.

The term HTHP is not clearly defined in literature. For example, Arpagaus et al. [2] label heat pumps with supply temperatures higher than 90 °C as high-temperature systems. The International Energy

Agency [3] defines classic industrial heat pumps as HTHPs with a heat source temperature of up to 40 °C and a heat sink temperature of up to 80 °C. In case of heat sink temperatures higher than 100 °C, the term very-high-temperature heat pumps is proposed. In this work, the classification according to the International Energy Agency is applied without the distinction between very-high-temperature and HTHPs.

A fast-growing amount of experimental studies of HTHP have been conducted. Exemplarily, Hassan et al. [4] examined an HTHP with the hydrochlorofluoroolefin (HCFO) refrigerant R1233zd(E) and developed a simulation model. The HTHP was designed to operate at heat sink temperatures above 130 °C, with the possibility of varying the compressor speed from 500 rpm to 1500 rpm. This work aimed to reach a coefficient of performance (*COP*) of greater than 4 in every operating point and to find the boundary conditions to achieve this goal. In their study, Jiang et al. [5] used the same refrigerant and supply temperatures up to 100 °C. They reached a *COP* of 3.67 at a temperature lift of 50 K and developed a semi-empirical simulation model. Arpagaus and Bertsch

<sup>\*</sup> Corresponding author.

E-mail address: [jaromir.jessberger@uni-bayreuth.de](mailto:jaromir.jessberger@uni-bayreuth.de) (J. Jeßberger).

Nomenclature			
$c$	Price, €·kWh <sup>-1</sup>	$Q$	Thermal capacity, kW
$C$	Costs, €·kW <sub>th</sub> <sup>-1</sup>	$r$	Price increase factor
COND	Condenser	$T$	Temperature, °C
$COP$	Coefficient of performance	$t$	Time, a
DHN	District heating network	$\Delta T$	Temperature difference, K
ESP	Electronic submersible pump	$\Delta x$	Sensor uncertainty, %
EVAP	Evaporator	$\Delta y$	Combined uncertainty, %
FS	Full-scale uncertainty, %	<i>Subscripts</i>	
GWP	Global warming potential, CO <sub>2</sub> -eq.	Electr	Electricity
HCFO	Hydrochlorofluoroolefine	Geo	Geothermal
HEX	Heat exchanger	glide	Temperature glide
HFO	Hydrofluoroolefine	HP	Heat pump
HTHP	High-temperature heat pump	Inv	Investment
IHX	Internal heat exchanger	lift	Temperature lift
$LCOH$	Levelized costs of heat	ob	Period under consideration
$Losses_{el}$	Electrical losses, %	prod. well	Geothermal production well
$Losses_{th}$	Thermal losses, %	reinjection	Geothermal reinjection
ODP	Ozone depletion potential, R-11-eq.	rel	relative
OR	Operating range uncertainty, %	return	Return mass flow
$p$	Pressure, bar	service	Service life
$P$	Electrical power, kW	sink	Heat sink
$q$	Interest rate	source	Heat source
		supply	Supply mass flow

[6] made an experimental comparison between R1224yd(Z) and R1233zd(E) in an HTHP. The laboratory HTHP shows a thermal output of 10 kW, and the performance was examined at different temperature lifts.

Mateu-Royo et al. [7] investigated the possibility of using different HCFOs instead of R245fa in HTHP cycles. R1224yd(Z) and R1233zd(E) are proving to be good alternatives. The results are also evaluated from an environmental point of view and show the potential of a CO<sub>2</sub>e-emission reduction of up to 57.3 % compared to conventional fossil fuel boilers. Based on this presented test rig, Navarro-Esbri et al. [8] developed a simulation model for refrigerant mixtures and evaluated it in a techno-ecological way. The results show that with a carbon emission factor of the electricity mix lower than 0.35 kgCO<sub>2</sub>e/kWh, HTHPs can reduce emissions compared to fossil fuel boilers. Brendel et al. [9] investigated high-glide refrigerant mixtures experimentally and showed a  $COP$  improvement compared to the best-performing hydrofluoroolefins (HFO)/HCFO of 14 %. Zhang et al. [10] demonstrated the feasibility of a new binary refrigerant mixture BY-5. The experimental results were used to validate a simulation model and showed the potential for supply temperatures up to 135 °C. The focus of the experimental studies is, therefore, on efficiency or supply temperature improvements as well as the investigation of different refrigerant mixtures.

The corresponding heat pump market is also growing significantly. In this context, Arpagaus [11] identified already 26 commercially available HTHPs with maximum supply temperatures above 90 °C, and the investment costs vary between 100 €/kW and 1000 €/kW [12]. Overall, market-ready technologies achieve heating capacities between 20 kW and 20 MW. Jiang et al. [13] published a review of the state of the art of HTHPs. They stated four suggestive prospects: low-GWP refrigerants, supply temperature higher than 100 °C, heating capacity higher than 1 MW and  $COPs$  over 4 at a temperature lift of 40 K.

Next to technical and thermodynamic aspects, several techno-economic analyses of HTHPs combined with industrial systems or district heating networks (DHN) have also been published. Mateu-Royo et al. [14] investigated the integration of HTHPs into DHNs. The DHN can be used as a heat sink and a heat source in their work. It is used as a heat sink when waste heat from a supermarket refrigeration system can

be used and as a heat source when industrial customers require heat. Arslan et al. [15] evaluated the combination of existing DHN with thermal energy storages and heat pumps. They conducted a multi-objective parameter optimisation to obtain a high performing combination of different variables like refrigerant and phase change material. The combination of geothermal heat source and large scale heat pumps was also examined by Jensen et al. [16], to identify the most suitable system configuration of two heat pumps connected in series. Kosmadakis et al. [17] investigated the integration into industrial processes and, thereby, the upgrade of waste heat up to 150 °C. The authors also examined different plant configurations like a simple HTHP cycle, the use of an internal heat exchanger and two-stage compression. Sartor et al. [18] investigated the integration into DHN with a focus on steam production and the behaviour of the  $COP$  of the HTHP. Deng et al. [19] investigated the combination of medium-deep geothermal boreholes with heat pumps focusing on optimising the system for supply temperatures up to 55 °C. Dumont et al. [20] examined the integration of HTHPs in the food and beverages industry. Their results indicated that HTHPs could meet 12 TWh/a of process heat demand in the German food and beverages industry. The combination of geothermal energy systems and HTHPs or large-scale heat pumps was investigated in different aspects. Arslan et al. [21] evaluated the combination of thermal energy storage and heat pumps for the peak load coverage in geothermal district heating systems from a thermodynamic, economic and environmental point of view. Kim et al. [22] designed an absorption/compression heat pump with a refrigerant mixture of ammonia and water to upgrade geothermal heat at 50 °C up to 90 °C with a simultaneous cold supply at 20 °C. Lu et al. [23] also analysed the potential of medium depths with the aim of steam generation by using a heat pump with a flash tank system. They compared different refrigerants with constant boundary conditions to identify the optimal system temperatures and refrigerant from a technical point of view. Wang et al. [24] developed a numerical deep borehole heat exchanger model to give guidance for the design of deep borehole heat exchangers in terms of structural and geological parameters. Wang et al. [25] also analysed such a system in a field application and proved the potential of medium-depth geothermal heat pump systems in cold regions for building heating. The peak load coverage and the supply temperature increase in

medium depths have been investigated by Jeßberger et al. [2]; both applications can reduce the Levelized costs of heat (LCOH) compared to oil and gas boilers. The sensitivity analyses showed that the electricity price has the most significant impact on the LCOH, followed by the COP and the full load hours. The literature overview illustrates that geothermal systems including large-scale heat pumps is a relevant research topic. However, part load behaviour of those heat pumps as well as the peak load coverage by heat pumps is mostly neglected in present studies. So far, published experimental investigations are mainly focussed on a high temperature lift or efficiency increase. This results in a significant research gap concerning the integration of HTHPs into geothermal systems under consideration of the part load behaviour, to represent a realistic system performance.

So, this study will carry out an experimental investigation of the part load behaviour of a high temperature heat pump. The test rig is a HTHP with a thermal output of 35 kW and a supply temperature of up to 130 °C. The working medium is the HCFO refrigerant R1233zd(E), which has low global warming potential (GWP) and ozone depletion potential (ODP). The conducted measurement series are analysed both at system and component level. The experimental investigation of part load behaviour and the influence of varying temperature lifts are implemented in the techno-economic models of the geothermal heating plant. Thereby, the upgrade of existing geothermal heating plants by decreasing the reinjection temperature of the thermal water is investigated. In contrast to previous investigations [26], the costs of the geothermal system are neglected to follow the approach of upgrading existing geothermal heating plants by means of the integration of large-scale heat pumps. The current geothermal heating capacity only in Bavaria leads to an amount of 1110 GWh heat per year [27], and this study shows the potential of using the already installed capacity as a possible heat source by using field data of one year of an existing heating plant combined with experimental data from the test rig. This makes it possible to expand the heat supply without additional geothermal development.

In the following chapters, the methodology is presented, followed by a discussion of the results of the experimental investigations and the

techno-economic analyses.

## 2. Methodology

In this chapter, the heat pump test rig is described, and the measurement procedure and evaluation methodology are continued. Subsequently, the boundary conditions of the presented case study, as well as the techno-economic methods, are presented.

### 2.1. Experimental setup

In order to provide reliable part load and off-design characteristics, a test rig of a HTHP with a thermal capacity of 35 kW is analysed. The experimental setup was initially introduced in 2022 [28] and is analogous to the experimental setup presented in the work of Jeßberger et al. [26,29]. As working fluid *trans*-1-Chloro-3,3,3-trifluoropropene (R1233zd(E)) is used. This HCFO has a GWP of 1 CO<sub>2</sub>e and an ODP of 0.00034 R-11e [30]. The flow chart is presented in Fig. 1. All pipes and heat exchangers are insulated to minimise the system's heat losses. In the following section, the heat pump circuit is described based on the flow chart. At state point 1, the suction gas enters the reciprocating piston compressor and is compressed and superheated in state point 2. A software-controlled frequency converter is used to vary the compressor speed from 758 rpm up to 2100 rpm to investigate the part load behaviour of the HTHP. From the outlet of the compressor, the refrigerant flows through the oil separator to separate the entrained oil and ensure optimum heat transfer in the condenser. Here, the working fluid releases thermal energy during condensation, and exits subcooled at state point 4. A software-controlled frequency converter is used to vary the compressor speed from 758 rpm up to 2100 rpm to investigate the part load behaviour of the HTHP. From the outlet of the compressor, the refrigerant flows through the oil separator to separate the entrained oil and ensure optimum heat transfer in the condenser. Here, the working fluid releases thermal energy during condensation, and exits subcooled at state point 4.

After passing the liquid tank, the subcooled working medium enters the internal heat exchanger (IHx) and is coupled to the outlet stream of the evaporator (state point 9 to 1) in order to ensure sufficient superheating of the suction gas. Concerning the high-pressure side, the expansion valve leads to an isenthalpic expansion from state point 8 to state point 9. In the following, the refrigerant gets evaporated and superheated by 5 K.

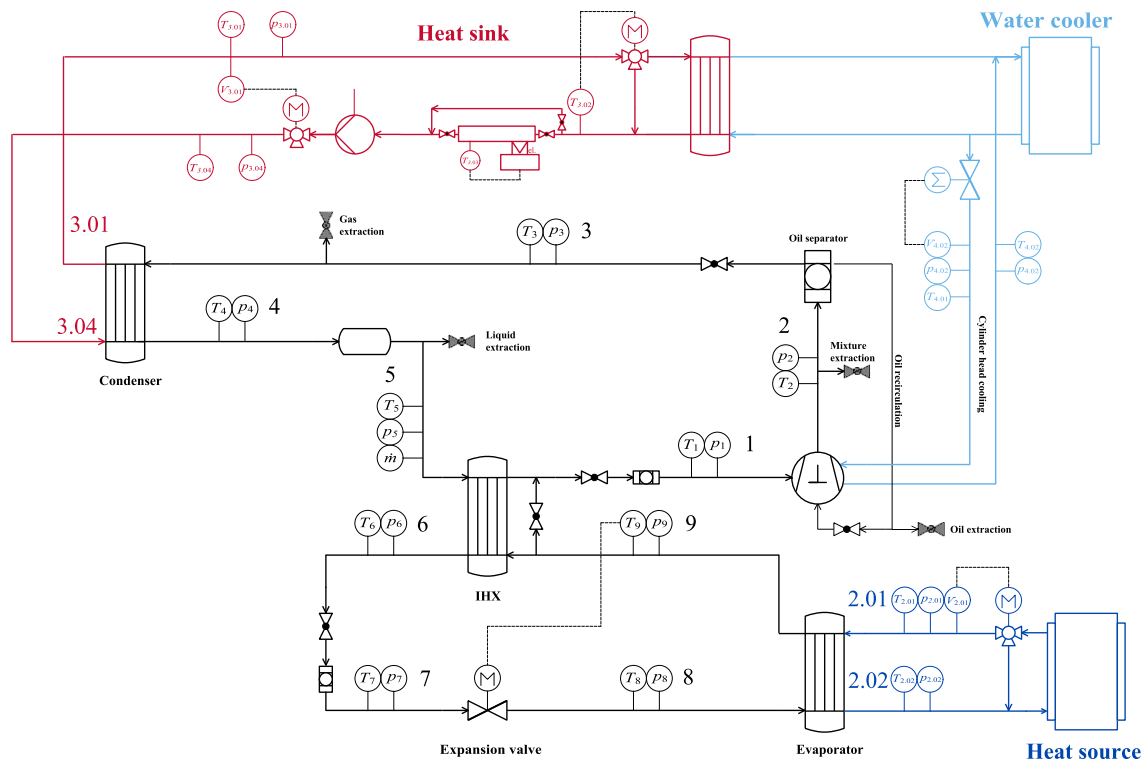


Fig. 1. Flow chart of the HTHP test rig.

The heat source is simulated by a tempering device, uses water as a medium, and the temperatures and the volume flow rate can be controlled software-based. A primary water circuit is used as a heat sink. The pump and bypass valve control the heat sink outlet temperature ( $T_{3,01}$ ), and the bypass valve after state point 3.1 controls, in combination with a heating device, the inlet temperature of the condenser ( $T_{3,04}$ ).

In addition, the test rig enables the following analysis and plant configuration:

- Sampling points for liquid, gaseous and oil-refrigerant mixtures.
- Variable internal heat exchanger surface by using a bypass valve.
- Water-cooled cylinder heads for compressor waste heat utilisation (see also Jeßberger et al. [31]).

### 2.2. Measurement procedure and error analysis

To carry out the techno-economic analysis with experimental performance data of the heat pump, the yearly mean temperatures of the district heating network (see Chapter 2.3) are used to simulate the base scenario of the heat pump performance. Additionally, the temperature lift ( $\Delta T_{lift}$ ) is varied by increasing the supply temperature from 70 °C to 100 °C in 5 K steps. Using fixed temperatures from the base case, the compressor speed is used to simulate the required flexibility and to vary the thermal power. Each operating point is measured in a steady state over a period of 10 min.

For the conducted experiments, the steady-state conditions are defined according to a change in the discharge temperature ( $T_{1,02}$ ), and the heat sink temperatures ( $T_{3,01}$  and  $T_{3,04}$ ) differ in a range below 1.5 K over a period of 10 min. Fig. 2 illustrates this steady state and shows the behaviour of the software-based PID controllers.

The measurement uncertainties are caused by the uncertainty of sensors and of the measurement board. It is essential to distinguish between a full-scale uncertainty (FS) and the operating range uncertainty (OR). FS refers to the maximum measurement deviation as a percentage of the total measurement range, while OR indicates the maximum deviation within the actual range used during a measurement. The reciprocal influence of the individual errors is calculated with the help of the Gaussian error propagation, according to DIN 1913-4 [32]. By calculating a parameter  $y$  as a function of different parameters  $x_i$ , the combined uncertainty  $\Delta y$  is defined as:

$$\Delta y = \sqrt{\left(\frac{\partial y}{\partial x_1} \Delta x_1\right)^2 + \left(\frac{\partial y}{\partial x_2} \Delta x_2\right)^2 + \dots + \left(\frac{\partial y}{\partial x_n} \Delta x_n\right)^2} \quad (1)$$

where  $\Delta x_i$  is the independent variable, generally provided by the

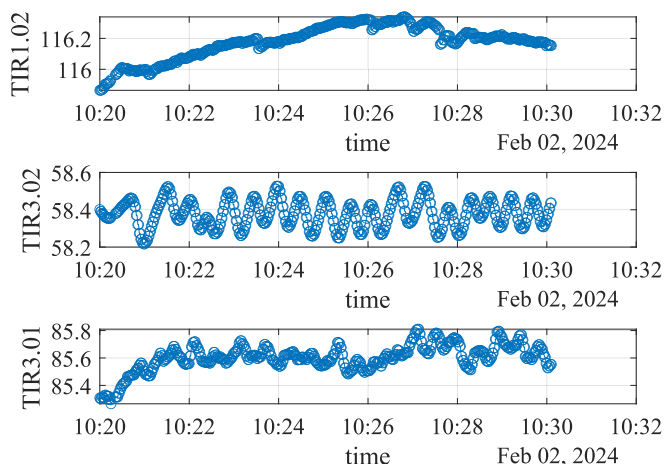


Fig. 2. Steady-state conditions for an exemplary operating point.

manufacturer and shown in Table 1.  $\Delta x_i$  comprises two components: the measurement uncertainty of the sensor itself and the error introduced by the measurement board.

Following this methodology, the base scenario regarding the mean temperatures of the DHN is investigated. To show the significant impact of varying temperature glides at the condenser and evaporator, their variation is also measured. The temperature glide is defined as the difference between the inlet and outlet of the water circuit on the condenser ( $T_{3,01} - T_{3,04}$ ) and evaporator ( $T_{2,01} - T_{2,02}$ ). This corresponds to a decreased return temperature of the DHN, and its effect on the COP of the heat pump could be quantified. The conducted measurement campaigns are summarised in Table 2 and show the great flexibility of the heat pump:

The following chapters introduce the existing geothermal heating plant as well as the potential concepts, investigated in this study.

### 2.3. Geothermal energy system

The investigated DHN is located in the south of Munich and has a maximum thermal capacity of 14 MW. The demand is served by two geothermal brines, which are using the hydrothermal reservoir of the South Bavarian Molasse Basin, see Fig. 3. The geothermal brine from two production wells (prod. well 1 and 2) is led into plate heat exchangers (HEX), release thermal energy to the DHN and get reinjected into the hydrothermal reservoir. The geothermal heating plant uses the geothermal brine for the base load coverage; the peak load coverage is realised by a fossil oil-based boiler, which is also implemented for redundancy. The geothermal boundary conditions like brine depth and required electrical power for electronic submersible pump (ESP) are published by Jeßberger et al. [26] and will not be focussed in this study. In contrast, the DHN and the reinjection temperature of the thermal water are discussed in detail in the following. Fig. 4 shows the geothermal water temperatures on the left-hand side as well as the temperature of the DHN on the right-hand side of the year 2015 in an hourly solution. Due to failure rates (for example, in the ESP), it can be seen that the geothermal source cannot be used to its full potential, which shows the necessity to improve the pump technology, reduce the downtimes and increase the service life.

The temperatures of the DHN are relatively constant, with a mean supply temperature of 85.6 °C and a mean return temperature of 58.2 °C. The fluctuating heat demand depending on weather conditions is served by varying the mass flow rate in the DHN, which is illustrated in Fig. 5.

Table 1  
Sensors and uncertainties.

Sensor	Type	Range	Sensor uncertainty	Board uncertainty
Temperature	Omega, PR-22-3-100-1/3-M3-100-M12	-30 °C to 350 °C	$dT = \pm (1/3 \cdot (0.30 \text{ °C} + 0.005 \cdot T))$	$\pm 0.15 \text{ °C}$
Pressure	Omega, PAA23SY-C-5-M12, 5 bar abs.	-1 bar to 5 bar	$\pm 0.7 \text{ \% FS}$	$\pm 0.76 \text{ \%}$
Pressure	Omega, PAA23SY-C-20-M12, 20 bar abs.	-1 bar to 20 bar	$\pm 0.7 \text{ \% FS}$	$\pm 0.76 \text{ \%}$
Mass flow refrigerant	Endress + Hauser, Proline Promass 40E	0 kg/h to 18,000 kg/h	$\pm 0.5 \text{ \% OR}$	negligible
Volume flow water circuits	Siemens, SITRANS FM MAG 3100P/5100 W	-	$\pm 0.4 \text{ \% OR}$ $\pm 1 \text{ mm/s}$	negligible
Electrical Power	-	-	$\pm 0.7 \text{ \% OR}$	negligible

**Table 2**  
Conducted measurement campaigns on the HTHP test rig.

Campaign	$T_{sink, in}$	$T_{sink, out}$	$T_{source, in}$	$T_{source, out}$	Compressor speed
Part load	58 °C	85.6 °C	68 °C	45 °C	758–2100 rpm
$\Delta T_{lift}$	58 °C	75 °C–100 °C	68 °C	45 °C	1517 rpm
$T_{glide,COND}$	30 °C–60 °C	85.6 °C	68 °C	45 °C	1517 rpm
$T_{glide,EVAP}$	58 °C	85.6 °C	68 °C	40 °C–5 °C	1517 rpm

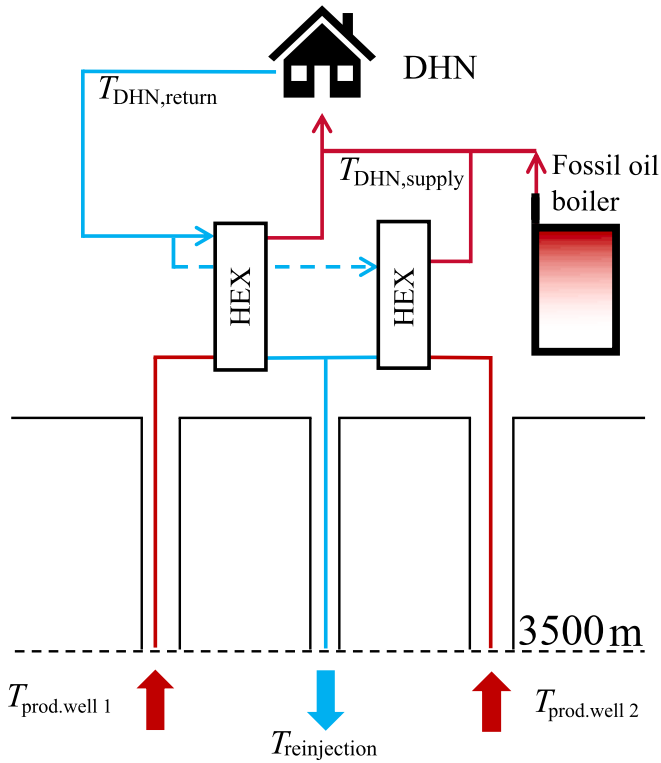


Fig. 3. Geothermal reference heating plant.

This graph also shows the need for peak load coverage, which is actually served by the fossil oil boilers (red part of the curve). With a share of 5.8 % of the demand of the DHN, the oil boiler has to supply 3 GWh/a.

Regarding Fig. 3 (left side), the mean reinjection temperature of the thermal water is 68 °C. This temperature level offers a vast potential to increase the thermal capacity of the heating plant by integrating a large-scale heat pump. All configurations shown in Fig. 6 decrease the

rejection temperature. In this study, a lower limit of 45 °C is defined. Configurations 1 and 2 both utilise the return temperature of the DHN as the inlet for the condenser of the heat pump. However, in configuration 1, the temperature is increased only to the extent that the thermal water can still be used for additional temperature increase. In contrast, configuration 2 involves the direct integration of the heat pump into the DHN. In configuration 3, the return mass flow rate of the DHN is fed into the geothermal heat exchanger and enters the heat pump as heat sink inlet temperature. Configuration 1 offers the smallest temperature lift of the heat pump, and configuration 2 requires the highest temperature glide at the condenser. Nevertheless, configurations 1 and 3 lead to larger geothermal heat exchangers due to the increased mass flow rate of the DHN, which is linked with new investment costs and a more extensive integration effort.

Configuration 2 requires the highest temperature lift but can be implemented in existing systems, provided that the DHN pipelines are

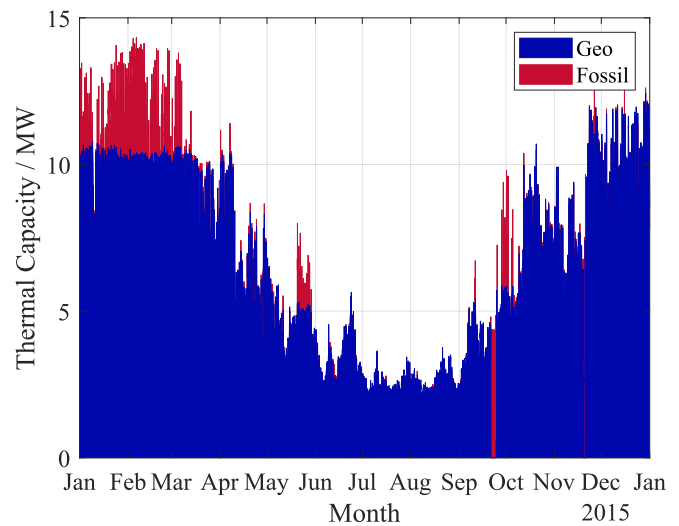


Fig. 5. Load profile of the DHN divided into the geothermal and fossil share.

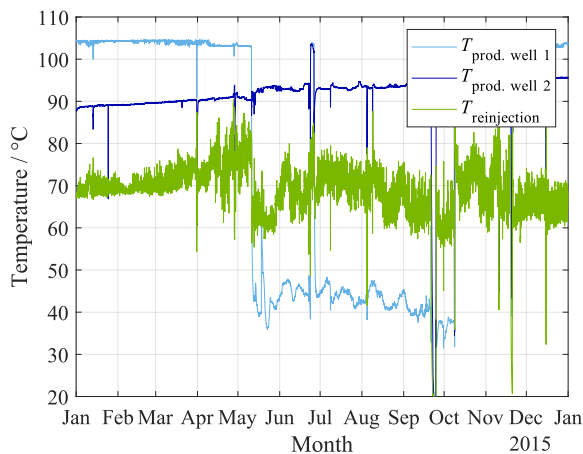
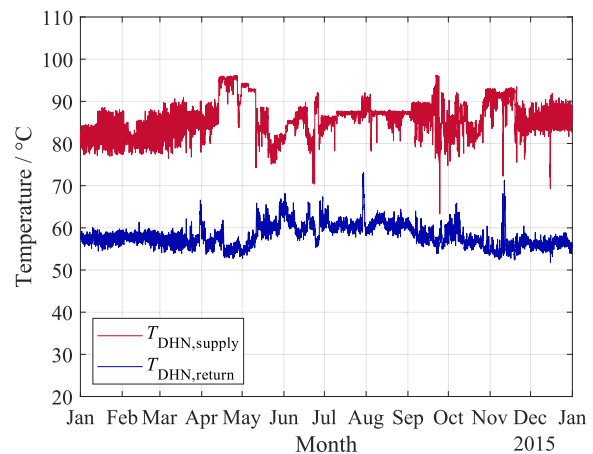


Fig. 4. Temperatures of the brine (left) and district heating network (right).



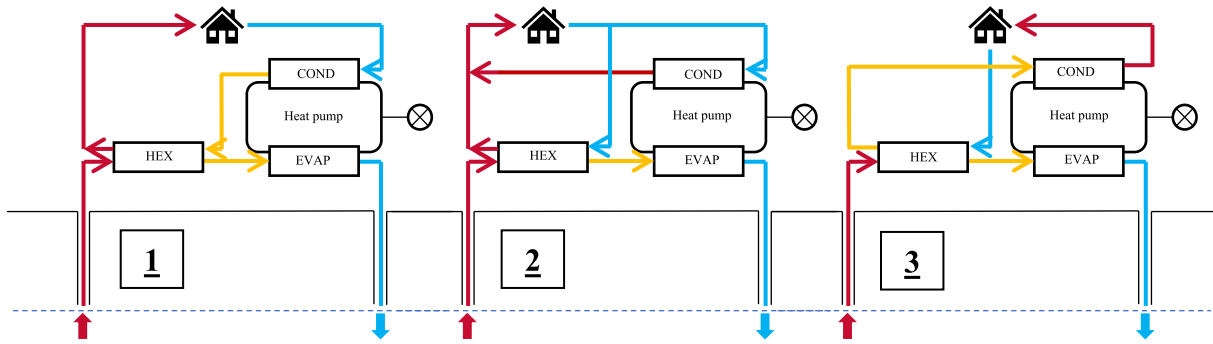


Fig. 6. Possible combinations of the geothermal heating plant with a large-scale heat pump.

able to handle an increased mass flow rate. In this study, configuration 2 is investigated to ensure comparability and transferability to other, in particular existing, geothermal heating plants.

#### 2.4. Thermodynamic and economic model

Besides the integration concept, it is necessary to define the boundary conditions of the techno-economic analyses. The boundary conditions are presented in Table 3 and are divided into constant values for the base scenario and due to the load profile fluctuating values.

The electricity price  $c_{\text{electr}}$  is taken from the first half year from 2022 for industrial customers in Germany [33]. For transferability to other countries, sensitivity analyses are carried out in the following chapter. The thermal and electrical losses of the heat pump are required to calculate the possible heat sink capacity (compare Jeßberger et al. [29]). The service life is used to take the replacement procurements into account depending on the period under consideration. The price increase factor  $r$  simulates the annual price increase caused by the inflation rate.

One of the most critical factors for the economic analysis is the efficiency of the heat pump, described by the  $COP$ . As mentioned in Chapter 2.2, the  $COP$  as a function of the temperature lift is investigated experimentally, followed by the analysis of the influence of varying compressor speed to investigate the part load behaviour. Using these experimental results, the  $COP$  is calculated as follows. First, the temperature lift is calculated:

$$\Delta T_{\text{lift}} = T_{\text{DHN, supply}} - T_{\text{Brine, return}} \quad (2)$$

Using the temperature lift, the  $COP$  as function of it leads to:

$$COP = a \cdot \Delta T_{\text{lift}}^2 + b \cdot \Delta T_{\text{lift}} + c \quad (3)$$

With  $a$ ,  $b$  and  $c$  as coefficients, determined by the measurements (see chapter 3.1). By using the  $COP$ , the thermal capacity of the heat pump can be calculated:

**Table 3**  
Boundary conditions for the techno-economic analysis.

Variable	Value
Input from the load profile	
$T_{\text{Geo}}$ [°C], $p_{\text{Geo}}$ [bar], $V_{\text{Geo}}$ [L/h]	fluctuating
$T_{\text{DHN}}$ [°C], $p_{\text{DHN}}$ [bar], $V_{\text{DHN}}$ [L/h]	fluctuating
Constant parameters	
Electricity price; $c_{\text{electr}}$	0.19 € kWh <sup>-1</sup> [33]
Period under consideration; $t_{\text{ob}}$	30 a
Thermal losses; $Losses_{\text{th}}$	3 % [29]
Electrical losses; $Losses_{\text{electr}}$	7 % [29]
Investment costs HP; $C_{\text{Inv,HP}}$	500 €-kWh <sub>th</sub> [112]
Service life HP; $t_{\text{service}}$	20 a [34]
Interest rate; $q$	1.05
Price increase factor; $r$	1.02

$$\dot{Q}_{\text{HP, sink}} = \frac{\dot{Q}_{\text{HP, source}}}{\left( \left( 1 - \dot{Q}_{\text{Losses, th}} \right) - \frac{1 + P_{\text{Losses, el}}}{COP} \right)} \quad (4)$$

With the thermal capacity the part load point regarding the heat pump capacity is calculated ( $Q_{\text{sink, rel}}$ ) and the experimental investigated part load behaviour is considered:

$$COP_{\text{part load}} = a \cdot \dot{Q}_{\text{sink, rel}}^2 + b \cdot \dot{Q}_{\text{sink, rel}} + c \quad (5)$$

Using Eq. (5), the relative change of the  $COP$  can be considered by using the quotient of the part load  $COP$  and the  $COP$  in the base scenario. So, the temperature lift depending  $COP$  changes, depending on the part load operating point.

The economic analysis is carried out using the annuity method regarding VDI 2067 [34]. The total annuity  $A_N$  refers to a regular annual payment. And depends on interest rate or period under consideration. Generally,  $A_N$  can be divided into the operation related costs (maintenance, personal, and labour costs), demand related costs (here electricity demand), other costs (neglected in this study), capital related costs (investments and replacement procurements) and incomes ( $I$ ).

$LCOH$  are calculated as follows:

$$LCOH = \frac{\text{total annuity } A_N \text{ [€} \cdot \text{a}^{-1}] - I}{\text{heat supplied [kWh} \cdot \text{a}^{-1}]} \quad (6)$$

The described economic evaluation is conducted considering in the boundary conditions of Table 3 and modelling the ESP-power consumption published by Jeßberger et al [29]. Subsidies are neglected in this study to ensure the transferability to other regions.

### 3. Results

In this chapter, the experimental and economic results are discussed. Table 4 shows the mean temperatures of the base scenario.

The focus is led on the base scenario of the existing heating plant. Subsequently, on the part load behaviour of the heat pump and the influence of the temperature glides in the condenser and evaporator. Following are the economic and simulated results of the integration of a heat pump with the behaviour of the test rig into an existing heating

**Table 4**  
Mean temperatures of the base scenario.

Variable	Value
Geothermal mean values	
$T_{\text{prod. well}}$ [°C]	68
$T_{\text{re injection}}$ [°C]	45
DHN mean values	
$T_{\text{DHN, supply}}$ [°C]	85
$T_{\text{DHN, return}}$ [°C]	58
$T_{\text{lift}}$ [K]	17

plant.

### 3.1. Experiments

As Fig. 4 shows, the supply temperature of the district heating network fluctuates between 70 °C and 95 °C depending on the operating strategy and the time and weather conditions. To deal with this input parameter in the techno-economic analyses, the influence of the changing temperature lift of the HTHP is investigated by the test rig. Fig. 7 shows the COP as a function of the temperature lift as well as a polynomial fit 2nd degree. The mean uncertainty of the COP for this measurement campaign is 0.09, with a maximum at low temperature lifts of 0.15 This is due to the increasing impact of the temperature sensor uncertainty at smaller temperature glides.

The mean temperature lift is around 17 K (see Table 4) and leads to a COP of 4.1. The figure shows that with increasing temperature lift, the COP decreases, which is caused by the higher required discharge temperature of the compressor. The result of the integration of heat pumps into DHNs is that a reduced supply temperature, reached by better-insulated pipes or better building standards, leads to higher system efficiency. The COP as a function of the temperature lift is also presented in Eq. (7):

$$COP = 0.000234 \cdot \Delta T_{lift}^2 - 0.049305 \cdot \Delta T_{lift} + 4.889506 \quad (7)$$

The next step is to investigate the part load behaviour of the heat pump, which is conducted by varying the compressor speed between the limits specified by the manufacturer. Fig. 8 shows the thermal capacity as a function of the compressor speed, underlying the base case boundary conditions (see Table 4). By changing the mass flow rates of the water circuits, depending on the thermal capacity, the base case temperatures were reached. The thermal capacity can be increased by increasing the compressor speed up to 122 % and decreased down to 56 %, shown on the left-hand side. The speed variation also infects the COP due to lower mass flow rates in the heat pump circuit; the relative heat exchanger surface changes and leads to an increase of the COP with decreasing thermal capacity at the heat sink.

The COP as function of the relative thermal capacity  $\dot{Q}_{sink,rel}$  can be described by Eq. (8).

$$COP = -0.000109 \cdot \dot{Q}_{sink,rel}^2 + 0.002114 \cdot \dot{Q}_{sink,rel} + 4.976554 \quad (8)$$

Using this equation, the part load behaviour of the heat pump can be considered in the techno-economic model.

Another aspect of the HTHP that is considered in the geothermal

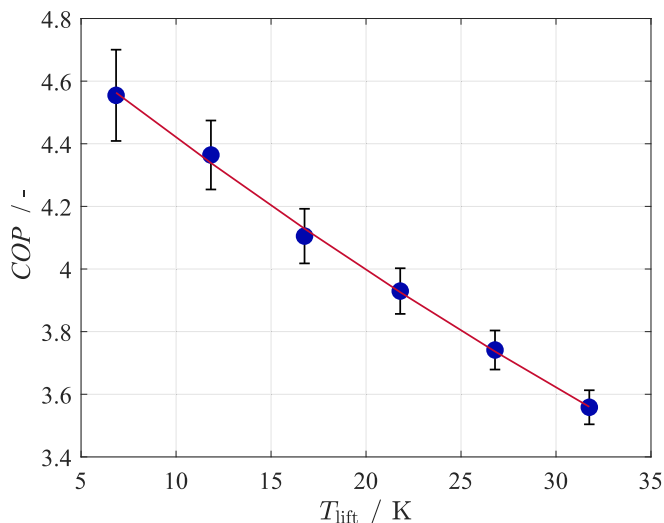


Fig. 7. COP as a function of the temperature lift.

system model is the influence of the temperature level of the DHN. The following measurement campaigns are carried out to show the impact of changing temperature glides on the water sides of the condenser and evaporator. On the condenser side, the temperature glide could be increased by adding low-temperature emitters, such as island DHNs with 4th or 5th generation standards, to the system. Conversely, the temperature glide at the evaporator could be decreased by increasing the thermal mass flow rate. Fig. 9 shows the COP as a function of the temperature glides (the difference between water inlet and outlet temperature) on the left for the condenser and on the right for the evaporator.

At the condenser, the supply temperature is kept constant at 86 °C, which corresponds to the mean temperature of the DHN supply temperature, according to Fig. 4. The return temperature is reduced to 30 °C, which leads to a temperature glide of 56 K. The increase of the temperature glide corresponds to the reduction of the return temperature of the DHN and shows that the COP can be increased by up to 6 %. The variation of the glide on the evaporator is only possible with a higher mass flow rate of the brine but shows a more significant impact. The increase leads to a higher evaporation temperature, which reduces the pressure ratio and the required electrical power. In the base scenario, the glide is 23 K. So, if an increase of the reinjection temperature by increasing the thermal mass flow rate is possible, the COP can be increased by up to 17 %, and the reinjection temperature would be increased to 56 °C. These results show the necessity of an intelligent and efficient system analysis. The results of the HTHP test rig with a thermal power of 35 kW are scalable to the MW-range as stated by Jeßberger et al. [35]. The upscaling of laboratory results was proven by comparing two laboratory HTHPs in combination with industrial data. Assuming the use of a reciprocating piston compressor combined with a frequency converter in the MW-range, the results are also adaptable to scale up the part load behaviour. In this context, the integration of large-scale heat pumps is investigated from a techno-economic perspective in the following chapter.

### 3.2. Techno-economic analysis

In respect to configuration 2, presented in chapter 2.3, two principal operational concepts exist. Both concepts using a fixed reinjection temperature of 45 °C. The results of the two possibilities are shown in Fig. 10. Firstly, the heat pump can be used instead of the peak load coverage system and is able to increase the capacity of the system simultaneously. In this case, the thermal capacity of the combined system (geothermal and heat pump) is shown in green on the left diagram. The red area shows the periods where the heat demand of the DHN is higher than the possible output of the combined system. This area corresponds only to 0.57 % (reduced from 5.8 %, compare Chapter 2.3) of the entirely provided thermal energy and is related to the downtimes of the ESPs and has to be served by the fossil peak load and redundancy system. Using this configuration in general, the thermal output can be increased from 52.5 GWh per year up to 109 GWh per year by this operational concept. The necessary fossil peak load coverage can be reduced from 3 GWh to 0.62 GWh per year. With more reliable ESP performance, the peak load coverage demand could be even entirely served by the heat pump. This should already be possible by now. However, this is conducted with available operational data of 2015 of the geothermal heating plant.

The second operational concept is to keep the existing heating plant unmodified and to add the possible extra heating capacity to the heat demand of the DHN, so the current peak load coverage is kept fossil to show the maximum possible upgrade potential. This method is presented in the right diagram of Fig. 10. The maximum capacity could be increased by up to 77.5 %, and the annual thermal output could be increased from 52.5 GWh up to 111 GWh per year.

The full load hours of the geothermal heating plant amount to 4115 h per year, and the full load hours of the heat pump lead to 3712 h per year in both operational concepts.

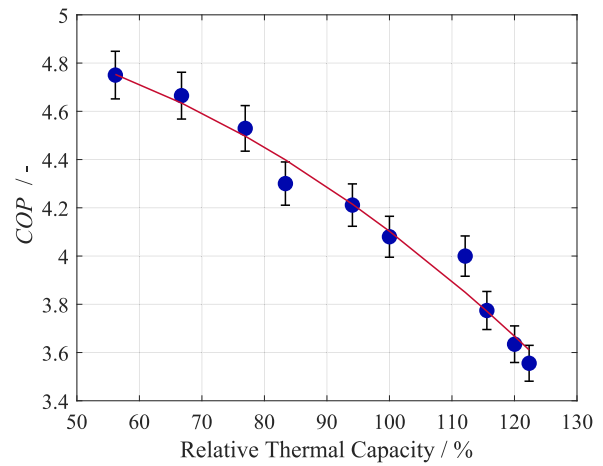
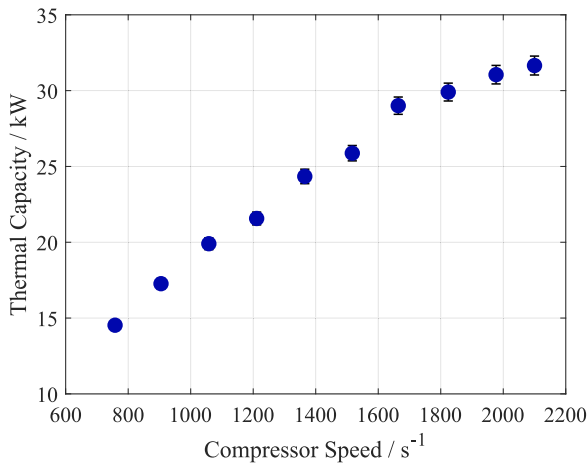


Fig. 8. Thermal capacity as function of the compressor speed and COP as function of the relative Thermal capacity.

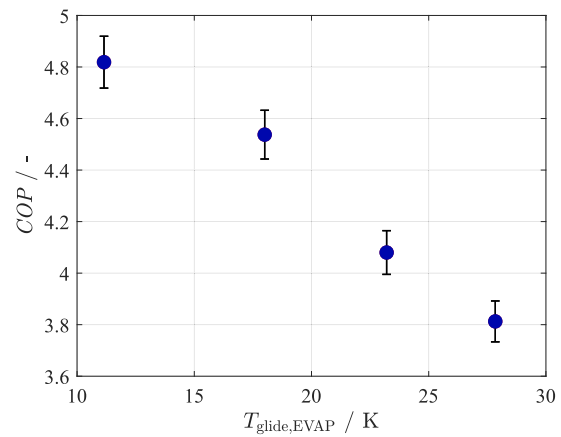
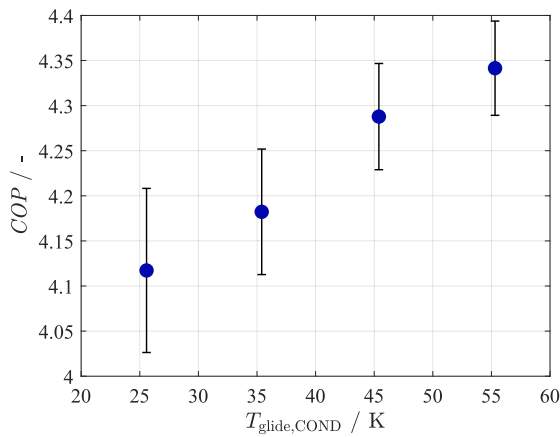


Fig. 9. COP as a function of the temperature glides on the condenser and evaporator.

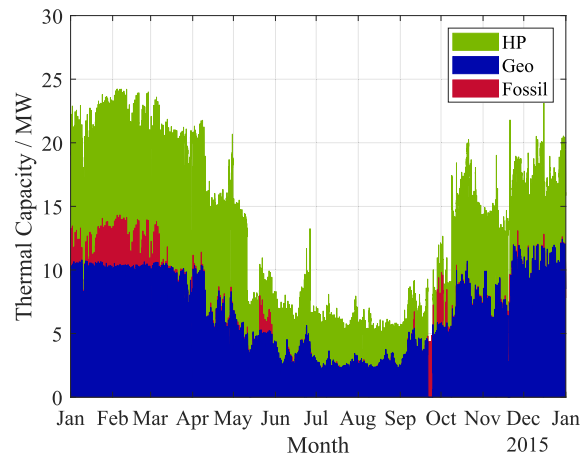
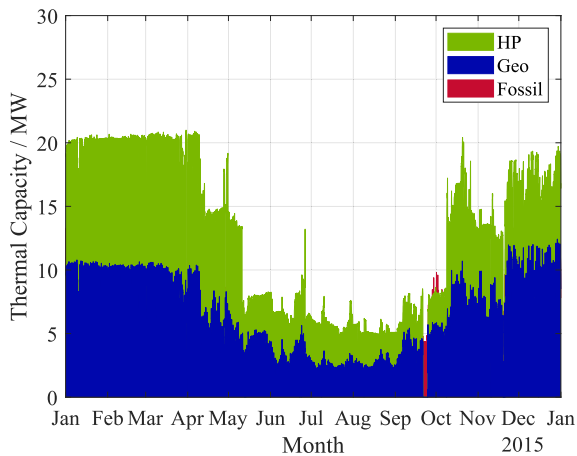


Fig. 10. Simultaneously peak load coverage and capacity lift (left) and potential for DHN capacity upgrade (right).

Concerning the economic results, Fig. 11 presents the annuities of the defined base scenario. The demand-related costs are 76 % of the overall annuity, the most crucial factor, and describe the required electricity demand. Followed by capital-related costs at 18 %, caused by the investment costs and the required replacement procurements and operation-related costs at 6 %, driven by maintenance and servicing. Using the method for the COP calculation (see Chapter 3.1) and the boundary conditions, the annuity method can be carried out, and the

LCOH can be calculated to 68 €/MWh.

The presented base scenario depends on a high number of boundary conditions specific to the given use case. For example, the electricity costs vary considerably from year to year and from country to country. Also, the investment costs and the COP of the heat pumps depend on boundary conditions given by the DHN and the geothermal source. To deal with that issue, sensitivity analyses are conducted for the most critical input parameters. Fig. 12 presents the corresponding results. On

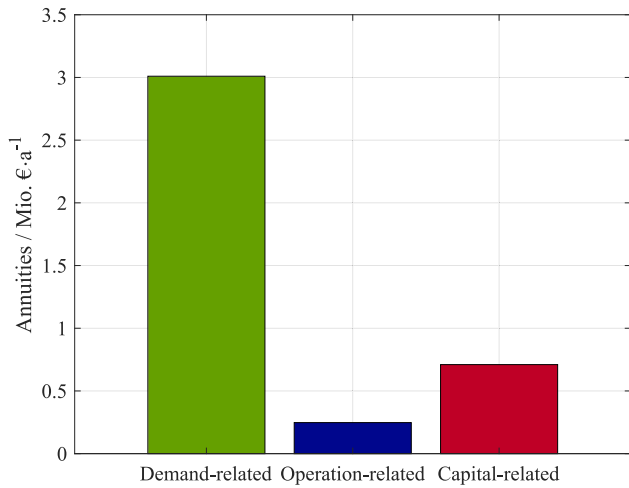


Fig. 11. Annuities of the base scenario.

the left-hand side, the variation of the *COP* and the electricity price, and on the right-hand side, the variation of the specific investment costs per kW thermal capacity and the period under consideration are displayed.

The *COP* is varied from 1.5 to 8 and shows an exponential influence on the *LCOH*. The red dot in the diagrams marks the base scenario, so by improving the *COP*, the *LCOH* can be reduced from 68 €/MWh down to 48 €/MWh, which corresponds to a reduction of 30 %. The German electricity price is one of the highest in the EU [36], so with an electricity price of 100 €/MWh instead of 195 € per MWh, the *LCOH* could be decreased by 39 %, down to 42 €/MWh. On the right diagram, the influence of the investment costs is presented. Fig. 11 already illustrates that the capital investment costs are not the major economic parameter. Therefore, the reduction based on specific investment costs of 200 €/kW is 17 %. The variation of the period under consideration is shown, to sensitise for its influence, because the replacement procurements as well as the price increasing factors have a significant impact on the results of techno-economic analyses. The results of an economic viability analysis must, therefore, be categorised differently depending on the period under consideration.

#### 4. Conclusion

In this study, the potential of upgrading an existing geothermal heating plant by integrating a large-scale heat pump was investigated. The geothermal boundary conditions, as well as the yearly demand of

the DHN, were used in an hourly solution over the period of one year as input parameters. The specific requirements, especially with the focus on different system temperatures, are investigated on a high-temperature heat pump test rig. An increase of the temperature lift leads to a decrease of the *COP*. A corresponding correlation based on the experimental data is implemented in the techno-economic model. Additionally, the part load behaviour of the heat pump is investigated by varying the compressor speed. The results show that with decreasing compressor speed, the *COP* increases, and the thermal capacity decreases. This behaviour is also implemented in the model and shifts, the temperature lift depending *COP*, up or down depending on the part load operating point. Finally, the influence of changing temperature glides at the condenser and evaporator has been investigated experimentally. Here, a decreasing temperature glide at the evaporator leads to a higher *COP* caused by the increasing evaporation temperature.

The economic analyses are carried out using the dynamic annuity method. The economic results of the analyses lead to an *LCOH* of 68 €/MWh. The costs of the system are dominated by base demand-related costs, which account for 76 % of the total annuity. Sensitivity analyses identified the *COP* and the electricity price as the most sensitive input parameters. As mentioned in Chapter 3.2, the thermal output per year can be more than doubled in the investigated system. With huge potential, the share of geothermal energy in the German heat supply could be increased highly without high drilling risks and investment costs. For example, the introduction stated that 1110 GWh/a geothermal heat is provided in Bavaria. This could be increased up to over 2000 GWh/a without new drillings, assuming that the preconditions are similar.

The study points out that the integration of large-scale heat pumps into geothermal heating plants has a huge potential to increase the share of renewable heat in the market. The study shows the possibilities not only in a technological way but also from an economic perspective, and the integration will be very beneficial for the plant operators. The results are transferable to other medium-deep geothermal energy systems, and the models can be adapted to the required boundary conditions. In conclusion, this work has shown that a new borehole is not immediately necessary when expanding a geothermal DHN. This means that complex reservoir management can be replaced by a comparatively simple above-ground upgrade.

The constraints inherent in this study primarily pertain to the upscaling of experimental findings from a laboratory setting to a larger scale. Moreover, adjusting the brine reinjection temperature necessitates compliance with both geological considerations and legal constraints contingent upon the specific location. In further work, the combination of large-scale heat pumps with a geothermal heating plant will be considered, and a multi-parameter optimisation will be carried out.

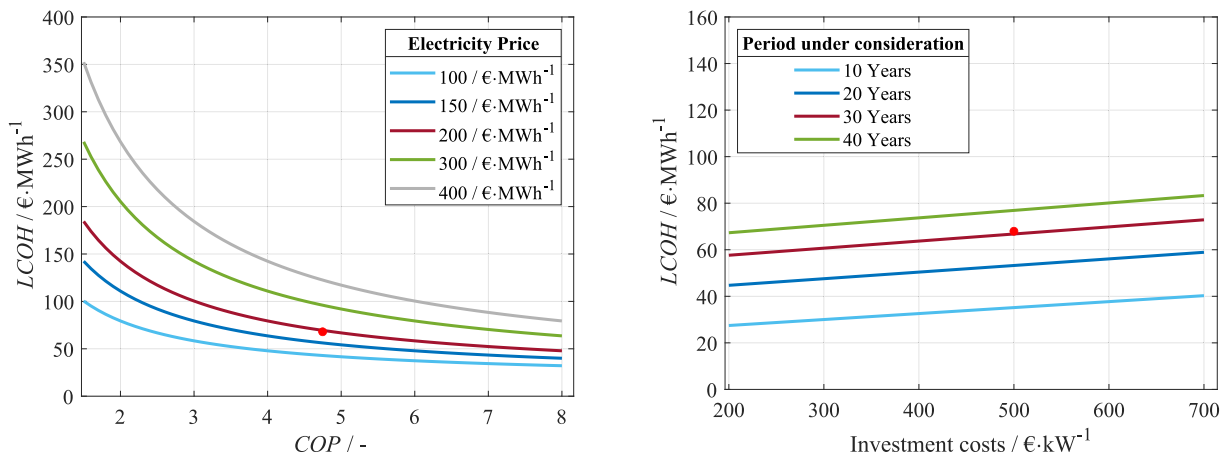


Fig. 12. Sensitivity analyses: Variation of *COP*, electricity price, period under consideration and investment costs.

## Declaration of competing interest

The authors declare that they have no known competing financial interests or personal relationships that could have appeared to influence the work reported in this paper.

## Data availability

Data will be made available on request.

## Acknowledgement

Funded by the Deutsche Forschungsgemeinschaft (DFG, German Research Foundation) – 491183248. Funded by the Open Access Publishing Fund of the University of Bayreuth. Additionally, we gratefully acknowledge the Bavarian State Ministry of Science and Arts within the framework of the “Geothermal Alliance Bavaria” project for funding.

## References

- [1] Eurostat, Heating and cooling from renewables gradually increasing, 2023, <https://ec.europa.eu/eurostat/de/web/products-eurostat-news/w/ddn-20230203-1>, accessed 09.02.24.
- [2] C. Arpagaus, F. Bless, M. Uhlmann, J. Schiffmann, S. Bertsch, High temperature heat pumps: market overview, state of the art, research status, refrigerants, and application potentials, *Int. Refrig. Air Cond. Conf.* (2018) 1–10.
- [3] International Energy Agency, Application of Industrial Heat Pumps: EA Industrial Energy-related Systems and Technologies Annex 13; IEA Heat Pump Programme Annex 35; Final Report Part 1, 35th ed., 2014.
- [4] A.H. Hassan, J.M. Corberán, M. Ramirez, F. Trebilcock-Kelly, J. Payá, A high-temperature heat pump for compressed heat energy storage applications: Design, modeling, and performance, *Energy Rep.* 8 (2022) 10833–10848.
- [5] J. Jiang, B. Hu, R.Z. Wang, T. Ge, H. Liu, Z. Zhang, Y. Zhou, Experiments of advanced centrifugal heat pump with supply temperature up to 100 °C using low-GWP refrigerant R1233zd(E), *Energy* 263 (2023) 126033.
- [6] C. Arpagaus, S. Bertsch, Experimenteller Vergleich von R1224yd(Z) und R1233zd(E) in einer Hochtemperatur-Wärmepumpe, *KI Kälte* (2020) 46–55.
- [7] C. Mateu-Royo, J. Navarro-Esbrí, A. Mota-Babiloni, F. Molés, M. Amat-Albuixech, Experimental exergy and energy analysis of a novel high-temperature heat pump with scroll compressor for waste heat recovery, *Appl. Energy* 253 (2019) 113504.
- [8] J. Navarro-Esbrí, A. Fernández-Moreno, A. Mota-Babiloni, Modelling and evaluation of a high-temperature heat pump two-stage cascade with refrigerant mixtures as a fossil fuel boiler alternative for industry decarbonization, *Energy* 254 (2022) 124308.
- [9] L. Brendel, Bernal S., C. Arpagaus, Widmayer P., D. Roskosch, A. Bardow, S. Bertsch, Experimental investigation of high-glide refrigerant mixture R1233zd(E)/R1234yf in a high-temperature heat pump, in: Proceedings of the 26th IIR International Congress of Refrigeration: Paris France, August 21–25, 2023.
- [10] Y. Zhang, Y. Zhang, X. Yu, J. Guo, N. Deng, S. Dong, Z. He, X. Ma, Analysis of a high temperature heat pump using BY-5 as refrigerant, *Appl. Therm. Eng.* 127 (2017) 1461–1468.
- [11] C. Arpagaus, Hochtemperatur-Wärmepumpen: Marktübersicht, Stand der Technik und Anwendungspotenziale, VDE VERLAG GMBH, Berlin, Offenbach, 2019.
- [12] C. Arpagaus, L. Brendel, S. Paranjape, F. Bless, M. Uhlmann, S. Bertsch, New Developments and Products for Supply Temperatures above 100 °C, 2023.
- [13] J. Jiang, B. Hu, R.Z. Wang, N. Deng, F. Cao, C.-C. Wang, A review and perspective on industry high-temperature heat pumps, *Renew. Sustain. Energy Rev.* 161 (2022) 112106.
- [14] C. Mateu-Royo, S. Sawalha, A. Mota-Babiloni, J. Navarro-Esbrí, High temperature heat pump integration into district heating network, *Energ. Convers. Manage.* 210 (2020) 112719.
- [15] O. Arslan, A.E. Arslan, I. Kurtbas, Exergoeconomic and exergoenvironmental based multi-criteria optimization of a new geothermal district heating system integrated with thermal energy storage driven heat pump, *J. Build. Eng.* 73 (2023) 106733.
- [16] J.K. Jensen, T. Ommen, W.B. Markussen, B. Elmegaard, Design of serially connected district heating heat pumps utilising a geothermal heat source, *Energy* 137 (2017) 865–877.
- [17] G. Kosmadakis, C. Arpagaus, P. Neofytou, S. Bertsch, Techno-economic analysis of high-temperature heat pumps with low-global warming potential refrigerants for upgrading waste heat up to 150 °C, *Energ. Convers. Manage.* 226 (2020) 113488.
- [18] K. Sartor, V. Lemort, P. Dewallef, Improved district heating network operation by the integration of high-temperature heat pumps, *Int. J. Sustain. Energy.* 37 (2018) 842–856.
- [19] J. Deng, Y. Su, C. Peng, W. Qiang, W. Cai, Q. Wei, H. Zhang, How to improve the energy performance of mid-deep geothermal heat pump systems: Optimization of heat pump, system configuration and control strategy, *Energy* 285 (2023) 129537.
- [20] M. Dumont, R. Wang, D. Wenzke, K. Blok, R. Heijungs, The techno-economic integrability of high-temperature heat pumps for decarbonizing process heat in the food and beverages industry, *Resour. Conserv. Recycl.* 188 (2023) 106605.
- [21] O. Arslan, A. Ergenekon Arslan, T. Eddine Boukelia, Modelling and optimization of domestic thermal energy storage based heat pump system for geothermal district heating, *Energy. Build.* 282 (2023) 112792.
- [22] M. Kim, Y.J. Baik, S.R. Park, K.C. Chang, H.S. Ra, Design of a high temperature production heat pump system using geothermal water at moderate temperature, *Curr. Appl Phys.* 10 (2010) S117–S122.
- [23] Z. Lu, Y. Gong, Y. Yao, C. Luo, W. Ma, Development of a high temperature heat pump system for steam generation using medium-low temperature geothermal water, *Energy Procedia* 158 (2019) 6046–6054.
- [24] X. Wang, Y. Su, G. Liu, L. Ni, Numerical investigation of the deep borehole heat exchanger in medium-depth geothermal heat pump system for building space heating, *Energy. Build.* 304 (2024) 113874.
- [25] X. Wang, T. Zhan, G. Liu, L. Ni, A field test of medium-depth geothermal heat pump system for heating in severely cold region, *Case Stud. Therm. Eng.* 48 (2023) 103125.
- [26] J. Jeßberger, F. Heberle, D. Brüggemann, Integration of high-temperature heat pumps into geothermal energy systems, in: 10th HEAT POWERED CYCLES Conference, 2023, pp. 16–30.
- [27] Energieatlas Bayern, Tiefe Geothermie: Zahlen & Fakten, [https://www.energieatlas.bayern.de/thema\\_geothermie/tiefe/daten](https://www.energieatlas.bayern.de/thema_geothermie/tiefe/daten).
- [28] J. Jeßberger, F. Heberle, D. Brüggemann, Integration von Hochtemperatur-Wärmepumpen in erneuerbare Energiesysteme, in: DKV Tagungsband, 2022.
- [29] J. Jeßberger, F. Heberle, D. Brüggemann, Integration of high temperature heat pumps into geothermal systems, in: EGC – European Geothermal Congress, 2022.
- [30] IPCC, Climate Change 2014: Synthesis Report. Contribution of Working Groups I, II and III to the Fifth Assessment Report of the Intergovernmental Panel on Climate Change, Geneva, Switzerland, 2014.
- [31] J. Jeßberger, F. Heberle, D. Brüggemann, Experimental investigations of water-cooled cylinder heads in a high temperature heat pump cycle, in: High-Temperature Heat Pump Symposium, 2024.
- [32] Deutsches Institut für Normung e.V., Grundlagen der Meßtechnik: Teil 4: Auswertung von Messungen Meßunsicherheit, Beuth Verlag GmbH, Berlin ICS 17.020, 1999.
- [33] Statistisches Bundesamt, Daten zur Energiepreisentwicklung DESTATIS, 2023, <https://www.destatis.de/DE/Themen/Wirtschaft/Preise/Publikationen/Energiepreise/energiepreisentwicklung-pdf-5619001.html>, accessed 5 February 2024.
- [34] Verein Deutscher Ingenieure, Wirtschaftlichkeit gebäudetechnischer Anlagen, Beuth Verlag GmbH, Berlin, 2012.
- [35] J. Jeßberger, C. Arpagaus, F. Heberle, L. Brendel, S. Bertsch, D. Brüggemann, Experimental investigations of upscaling effects of high-temperature heat pumps with R1233zd(E)(fr)Études expérimentales des effets d'échelle des pompes à chaleur haute température au R1233zd(E), *Int. J. Refrig.* (2024).
- [36] Eurostat, Electricity price for industrial customers, 2023, [https://ec.europa.eu/eurostat/statistics-explained/index.php?title=Electricity\\_price\\_statistics#Electricity\\_prices\\_for\\_non-household\\_consumers](https://ec.europa.eu/eurostat/statistics-explained/index.php?title=Electricity_price_statistics#Electricity_prices_for_non-household_consumers), accessed 09.02.24.